Title
Prediction and measurement of mass, heat, and momentum transport in a nonreacting turbulent flow of a jet in an opposing stream

Journal
Journal of Fluids Engineering, Transactions of the ASME, 103(1)

ISSN
0098-2202

Authors
Elghobashi, SE
Samuelsen, GS
Wuerer, JE
et al.

Publication Date
1981

DOI
10.1115/1.3240760

S. E. Elghobashi
Assistant Professor.
Mem. ASME

G. S. Samuelsen
Associate Professor.
Mem. ASME

Mechanical Engineering,
University of California,
Irvine, Calif.

J. E. Wuerer
Senior Scientist,
Spectron Development Laboratories, Inc.,
Costa Mesa, Calif.

J. C. LaRue
Assistant Research Engineer and Lecturer,
University of California,
San Diego, Calif.

Prediction and Measurement of Mass, Heat, and Momentum Transport in a Nonreacting Turbulent Flow of a Jet in an Opposing Stream

The paper addresses the measurement and prediction of heat, mass, and momentum transport in a confined axisymmetric turbulent nonreacting flow of a jet in an opposing stream. The predictions are obtained by solving numerically the conservation equations of the mean flow and the transport equations of the kinetic energy of turbulence and its dissipation rate and the mean square temperature fluctuations. The predicted velocity field is in agreement with the experiment, but the predicted scalar fields point to the need of examining the employed model of a scalar turbulent diffusion.

Introduction

The present capabilities of methods available to predict turbulent, reacting flows with recirculation have been demonstrated in studies directed to the evaluation of combustor performance (e.g., [1–3]). The results, though encouraging, suggest that systematic testing is needed to validate the mathematical models employed by such methods. For example, well controlled experiments need to be conducted, and complexities need to be introduced one at a time. A major requirement of such an approach is to first test the performance of the models against the experiment in the absence of reaction and heat release.

In earlier work, tests for the description of mass and momentum transport have been conducted in the absence of reaction and heat release [4, 5]. The present investigation extends the tests to include the transport of heat.

The flow configuration consists of a turbulent pipe flow with an on-axis jet opposing the main flow (Fig. 1). A highly turbulent recirculation zone results from the interaction of the two flows. The flowfield has distinctive features that make it particularly attractive from both experimental and analytical viewpoints. First, the recirculation zone is not attached to solid walls. Secondly, the range of velocity gradients, turbulence levels, and mixing lengths is increased over that offered by bluff bodies. The isolation of the recirculation zone from solid boundaries frees the analysis from complicated questions associated with the boundary condition specifications, while the extension of the range of turbulence

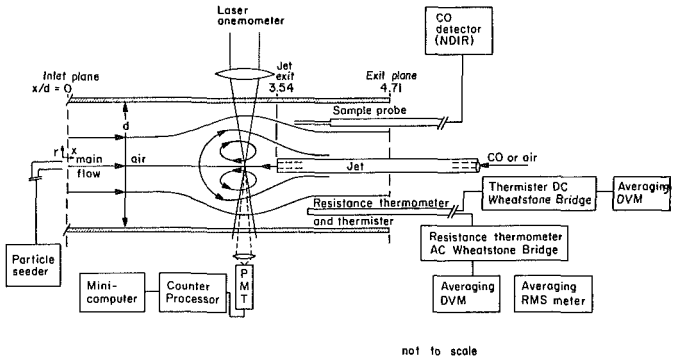

Fig. 1 Schematic of experimental apparatus

phenomena provides a broad test of the mathematical models involved in the flowfield predictions.

In the present case, the accuracy of the predicted mass transport was assessed by comparing the predicted and measured axial and radial transport of a tracer species, carbon monoxide, which was introduced through the jet with experimental data. Momentum transport was assessed by comparing predicted values of velocity and turbulence intensity with their measured values. Heat transport was assessed by heating the jet and comparing predicted values of mean and RMS temperature with experimentally measured values.

Experiment

Geometry. The experimental apparatus (Fig. 1) consisted of a 51 mm inside diameter (3 mm wall) by 240 mm long cylindrical Vycor (transparent quartz) tube containing an

Contributed by the Fluids Engineering Division for publication in the JOURNAL OF FLUIDS ENGINEERING. Manuscript received by the Fluids Engineering Division, November 27, 1979.

Table 1 Operating conditions

Variable	Cold flow		Heated flow	
$U_{m,i}$ (m/s)	7.5	15	7.5	15
Mach No.	0.025	0.05	0.025	0.05
Re_i	25000	50000	25000	50000
$U_{m,j}$ (m/s)	135		153	
Mach, j	0.4		0.4	
Re_j	11000		12500	
T_i (K)	295		295	
T_j (K)	295		327	
Main flow fluid	air		air	
Jet flow fluid	CO		air	

opposing axisymmetric jet. The diameter of the jet was 1.3 mm and the jet exit was located at $x/d = 3.54$ (i.e., 180 mm from the inlet plane). The jet tube was a circular cylinder with an outside diameter of 6.4 mm. The exit plane of the tube was located at $x/d = 4.71$.

Operating Conditions. Table 1 summarizes the four experimental operating conditions considered in this study.

Velocity Measurements. Velocity measurements were made using a laser anemometer system. One thousand samples of instantaneous velocity were taken at each measurement point within the flowfield. These measurements allowed the subsequent determination of the time-mean and root mean square values of the axial velocity.

The laser anemometer system was operated in a differential doppler mode using forward scattered light collection. Two beams, split from a 15 mw helium-neon laser (Spectra-Physics Model 124B), were focused through a 250 mm lens to form a fringe spacing of 1.69 μm. A 40 MH frequency shift (TSI Model 915 Bragg Cell) was applied to one beam to resolve ambiguity of velocity direction over the wide dynamic range observed in the highly turbulent flow. Signal validation was obtained using a counter processor (Macrodyne Model 2098). The data were reduced by a minicomputer (DEC Model PDP 11/10). The main flow was seeded with approximately 1 μm sodium chloride particles. The jet was not seeded in the present experiment. Velocity measurements in the recirculation zone are therefore biased to the main flow within a region bounded by approximately $r/R < 0.3$ and $x/d > 2.5$.

Concentration Measurements. The local concentration of the CO tracer species was measured using a continuous probe sampling system in conjunction with a nondispersive infrared analyzer (Beckman Model 915BL). The probe was constructed of capillary tubing (1.25 mm O.D.) to minimize probe perturbation effects. This technique provided local time-averaged concentration measurements. The use of a tracer species having essentially the same molecular mass as that of the main flow avoided biasing errors associated with density fluctuations. Repeated measurements at the same nominal position in the flow indicated that the variation in CO measurement is less that 10%. The repeated measurements included the evaluation of probe perturbation by using independently three probes, each with a unique angle of approach to the sampling point (straight -0 deg, angle -90 deg, hook -180 deg).

Temperature Measurements. The temperature signals were obtained by means of 0.125 mm diameter glass coated thermisters and a 1.25 μm diameter resistance ("cold wire") thermometer. The cold wire were platinum and 0.48 mm in length for $U_{m,i} = 7.5$ m/s, and platinum $-$ 10 percent rhodium and 0.66 mm in length for $U_{m,i} = 15.0$ m/s. The cold wires were operated with a root mean square current of 255 microamperes.

Nomenclature

$C_\mu, C_1, C_2, C_{T1}, C_{T2}$ = constants in the turbulence model
d = diameter of the large tube
D = molecular diffusivity
f = fluctuation of F
F = mass fraction of carbon monoxide
F_v = volume fraction of carbon monoxide
G = production of the turbulence kinetic energy
h = enthalpy fluctuation
H = stagnation enthalpy
k = kinetic energy of turbulence = $\frac{1}{2}\overline{u_i u_i}$
p = mean static pressure
r = radial distance
R = radius of the large tube
T = time-mean temperature
T' = RMS temperature fluctuation
U_i, u_i = mean and fluctuating velocities (tensor notation) in direction x_i
x_i = distance coordinate
Γ = thermal diffusivity of the fluid
δ_{ij} = Kronecker delta
ϵ = rate of dissipation of turbulence kinetic energy, k
Θ = time-mean temperature difference = $T - T_i$
Θ_{max} = max time-mean temperature difference = $T_j - T_i$
μ_{eff} = effective eddy viscosity
ν = kinematic viscosity of the fluid
ρ = fluid density
$\sigma_k, \sigma_\epsilon, \sigma_H, \sigma_T$ = turbulent Prandtl/Schmidt numbers
τ_{ij} = stress tensor

Subscripts

C.L. = center line
i = condition at the inlet of the large tube, except when used in tensor notation
j = condition at the jet exit, except when used in tensor notation
m = average axial velocity at a given axial location
max = maximum value

Superscripts

$'$ = fluctuating component
$\overline{\quad}$ = time-averaged value

The measurement of the mean and in particular the root mean square temperature fluctuations requires care and attention in the selection of the geometrical and operating characteristics of the sensor. For example, the sensor length must be much smaller than the length scales associated with the energy containing eddies so as to minimize the effects of spatial averaging [6] but the sensor length must be long enough so that sensor supports have a negligible effect on the sensor response [7-9]. The sensor current must be high enough so that there is a reasonable signal to noise ratio but the current must be low enough so that the sensitivity to velocity is negligible [10]. In addition, the sensor diameter must be small enough so that the corresponding frequency response is higher than that corresponding to the energy containing scales but must be large enough so that the sensor is mechanically robust.

The frequency response at 15 m/s of the thermister and associated d.c. bridge was estimated to be no more than 1Hz, while the frequency response of the cold wires was estimated to be about 1.5kHz [10]. The length scales and frequencies of the energy containing eddies are estimated to be half the radius of the main tube (i.e. 1.25 cm), which at a velocity of 15 m/s corresponds to a frequency of 1.2kHz. Thus the lengths of both sensors are small enough so as to permit the measurement of mean temperature while the length and frequency response of the cold wire permit the measurement of the root mean square temperature. The velocity sensitivity based on the results of reference [10] is estimated to be at most 3.0×10^{-3} °C (m/s) − 1. Typical errors in the mean and in the root mean square temperature are respectively 0.01 and 0.02 °C. Thus the error due to velocity sensitivity is negligible compared to the mean temperature which is nominally 1 °C.

The reduction in the measured root mean square temperature relative to the true mean square temperature due to heat conduction to the sensor support is estimated to be less than 12 percent [8].

The accuracy of the measured mean and root mean square is also related to the averaging and data reduction procedure. Both sensors and associated electronics were directly calibrated as a function of temperature so that the output was directly interpretable in terms of temperature, $\Theta(x,y,z,t)$, measured relative to the fluid temperature in the undisturbed pipe flow. The mean temperature from both the thermister and resistance thermometers was obtained by means of an averaging voltmeter, while the root mean square temperature was obtained by means of an averaging root mean square voltmeter. Averaging times of 10-30 seconds were used to obtain the statistical quantities reported herein. These averaging times correspond to averaging of at least 3500 integral time scales which should be adequate so as to insure good statistical reliability. Repeated measurements at the same nominal position in the flow indicate that the variation in relative mean temperature is less that 15 percent and that of the root mean square temperature is less that 5 percent. The primary reason that the variance of the relative mean temperature is greater than that of the root mean square temperature is that the former is determined from the differences of two variables (T_i and T), which are the same order of magnitude, while the latter is obtained directly.

Consideration of all the sources of error discussed in the proceeding indicates that the error in the measured and root mean square temperature is less than 15 percent.

Mathematical Model

The Mean Flow Equations. The equations[1] which describe the conservation of mass, momentum, energy and inert species in a turbulent flow are, respectively:

$$\frac{\partial}{\partial x_i}(\rho U_i) = 0 \tag{1}$$

$$\frac{\partial}{\partial x_i}(\rho U_i U_j) = -\frac{\partial p}{\partial x_i} - \frac{\partial \tau_{ij}}{\partial x_i} \tag{2}$$

$$\frac{\partial}{\partial x_i}(\rho U_i H) = \frac{\partial}{\partial x_i}\left(\Gamma \frac{\partial H}{\partial x_i} - \rho \overline{u_i h}\right) \tag{3}$$

$$\frac{\partial}{\partial x_i}(\rho U_i F) = \frac{\partial}{\partial x_i}\left(D \frac{\partial F}{\partial x_i} - \rho \overline{u_i f}\right) \tag{4}$$

In equations (1) to (4), terms involving density fluctuations have been neglected. This is justified in the flows under consideration for the following reasons. In the isothermal case the molecular mass of carbon monoxide and air are almost equal. In the case of the heated jet, the difference between the inlet mean temperatures of the jet and the main flow represents only 10 percent of the main flow temperature.

For the axisymmetric geometry of Fig. 1, two momentum equations (for the axial and radial directions) are required. The five equations (1)-(4) form a closed set when τ_{ij}, $\overline{u_i h}$, and $\overline{u_i f}$, are known. This is discussed in the next section.

The Turbulence Model. In order to close the above set of equations the stress tensor τ_{ij}, and turbulent heat flux $\rho\,\overline{u_i h}$ and the inert species turbulent mass flux $\rho\,\overline{u_i f}$, are evaluated by means of the standard $k-\epsilon$ turbulence model. In this model, the components of τ_{ij} are calculated from the following algebraic relation:

$$\rho\,\overline{u_i u_j} = \frac{2}{3}\rho k\,\delta_{ij} - \mu_{\text{eff}}\left(\frac{\partial U_i}{\partial x_j} + \frac{\partial U_j}{\partial x_i}\right) \tag{5}$$

where

$$\mu_{\text{eff}} = c_\mu \rho\, k^2/\epsilon \tag{6}$$

In the foregoing equations k is the kinetic energy of turbulence ($k = 1/2\,\overline{u_i u_i}$) and ϵ is the rate of dissipation of that energy ($\epsilon = \nu\,(\partial u_i/\partial x_i)^2$). The spatial distribution of k and ϵ are obtained from the solution of the following transport equations:

$$\frac{\partial}{\partial x_i}(\rho\, U_i\, k) = \frac{\partial}{\partial x_i}\left(\frac{\mu_{\text{eff}}}{\sigma_k}\frac{\partial k}{\partial x_i}\right) + G - \rho\epsilon \tag{7}$$

$$\frac{\partial}{\partial x_i}(\rho\, U_i\, \epsilon) = \frac{\partial}{\partial x_i}\left(\frac{\mu_{\text{eff}}}{\sigma_\epsilon}\frac{\partial \epsilon}{\partial x_i}\right) + (C_1\, G - C_2\, \rho\epsilon)\frac{\epsilon}{k} \tag{8}$$

$$G = -\rho\,\overline{u_i u_j}\frac{\partial U_i}{\partial x_j} \text{ and} \tag{9}$$

C_1 and C_2 are constants.

The transport equation for the mean square fluctuation of temperature which is solved simultaneously with the above set of equations is:

$$\frac{\partial}{\partial x_i}(\rho\, U_i\, \overline{T'^2}) = \frac{\partial}{\partial x_i}\left(\frac{\mu_{\text{eff}}}{\sigma_T}\frac{\overline{\partial T'^2}}{\partial x_i}\right) + G_T - C_{T2}\,\rho\,\overline{T'^2}\,\frac{\epsilon}{k} \tag{10}$$

where

$$G_T = C_{T1}\,\mu_{\text{eff}}\left[\frac{\partial T}{\partial x_i}\right]^2 \tag{11}$$

and C_{T1} and C_{T2} are constants.

[1] The equations 1,2,3,4,7,8,10 are quoted here in terms of Cartesian tensors for compactness. Their cylindrical-polar coordinates form is used to obtain the present results.

Table 2

C_μ	C_1	C_2	σ_k	σ_ϵ	C_{T1}	C_{T2}	σ_T
0.09	1.43	1.92	1.0	1.09	2.8	1.4	0.9

The set of constants used in the turbulence models are given in Table 2.

The values of the first five constants are adopted from Launder and Spalding [11]. The value of C_{T1} was first obtained from comparisons with experimental data of concentration fluctuations in isothermal flows [12]. The value of C_{T2} adopted in [13] was 2; however, the value used here, 1.4, is consistent with the experimental data of the decay of scalar fluctuations in grid turbulence [14], [15].

The Boundary Conditions. To complete the mathematical formulation, boundary conditions must be specified along the boundaries of the integration domain. Along the symmetry axis, the radial gradient vanishes for all variables except the radial velocity which equals zero. The inlet velocity profiles for the main flow are specified from the experimental data; for the jet the profile is assumed to be of the plug type. The values of k and ϵ at the inlet planes are prescribed by specifying the intensity and the scale of turbulence at the inlet.

At the exit plane, it is assumed that the axial gradients for all variables are zero. Along the top cylindrical wall, the axial and radial velocities equal zero. The wall functions [1] are used to calculate the values of the generation and dissipation of k and ϵ at the near wall node based on the assumption of Couette flow.

The Numerical Solution Procedure. The set of equations (1-4), (7), (8), (10) described above, together with their boundary conditions, was solved by an iterative finite difference procedure based on the Simple algorithm of Patankar and Spalding [16], but modified for elliptic flows. The grid refinement tests were carried out using three nonuniform grids: 16×12, 25×12, and 25×20, where the larger number of nodes was in the axial direction. The 25×20 grid was employed for the computations presented here.

A typical CPU time required for achieving a converged solution (300 iterations) was 5 minutes on a DEC 10 computer (equivalent to CDC 6400). The convergence criterion employed is that the maximum residual R_ϕ is less than 10^{-4}, where R_ϕ = (convection + diffusion + source)/$\phi_{\text{reference}}$, and ϕ is the dependent variable solved for.

Results and Discussions

The experimental and predicted results are presented for the cold and heated flows at 15 m/s and 7.5 m/s inlet velocities in Figs. 2 through 8. These include radial profiles of the time-mean axial velocity, the distribution of kinetic energy of turbulence along the center line of the tube, the radial profiles of the time-mean and the RMS temperature, and radial profiles of CO volume-fraction.

The Time-Mean Axial Velocity. Figure 2 shows the radial distributions of $(U/U_{\text{C.L.},i})$ at two axial locations (x/d = 2.95, 3.15) for both the cold and heated flows with $U_{m,i}$ = 15 m/s. At these stations velocity measurements were obtained at radial locations of r/R equal to or greater that 0.2 due to the biasing adjacent to the center line that was caused by the absence of seeding in the jet. At these radial locations, the predicted velocities are in fair agreement with their experimental values.

The two velocity profiles of the cold flow indicate that the stagnation point along the centerline of the jet lies between the two stations of x/d = 2.95 and x/d = 3.15 where the normalized center-line velocity drops from 0.4 to −1.0. The

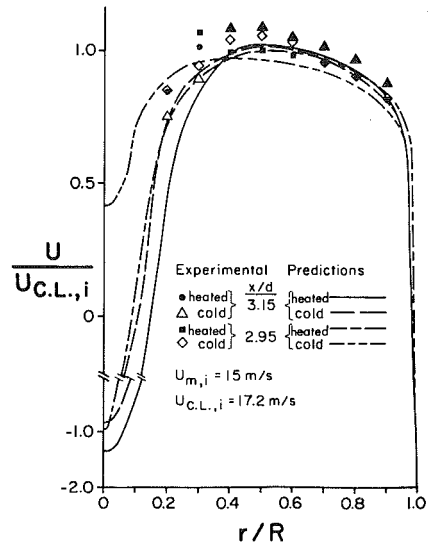

Fig. 2 Radial profiles of time-mean velocity (15 m/s)

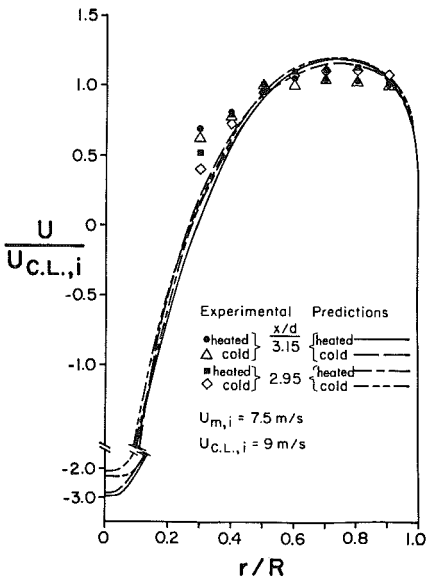

Fig. 3 Radial profiles of time-mean velocity (7.5 m/s)

respective profiles for the heated jet demonstrate that its stagnation point is located upstream the station of x/d = 2.95, i.e. the recirculation zone is longer for the heated than for the cold jet.

The predicted center line velocities for the heated flow attain larger negative values compared to their values in the cold flow. This is because the velocity of the heated jet is approximately 11 percent higher than that of the cold jet. The momentum of the jet is 21 percent and 27 percent, respectively, of that of the main flow for the cold and heated cases.

Figure 3 shows that radial distributions $U/U_{\text{C.L.},i}$ at the same axial stations for $U_{m,i}$ = 7.5m/s. The experiments and predictions depict similar behavior to that of the high velocity case, except that the magnitudes of the negative velocities at the centerline are much larger (almost twice as large) than

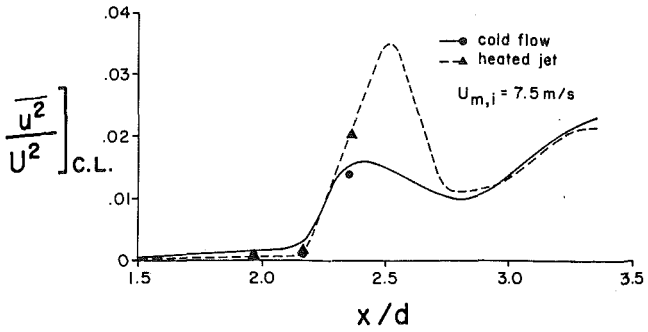

Fig. 4 Axial distribution of turbulence intensity

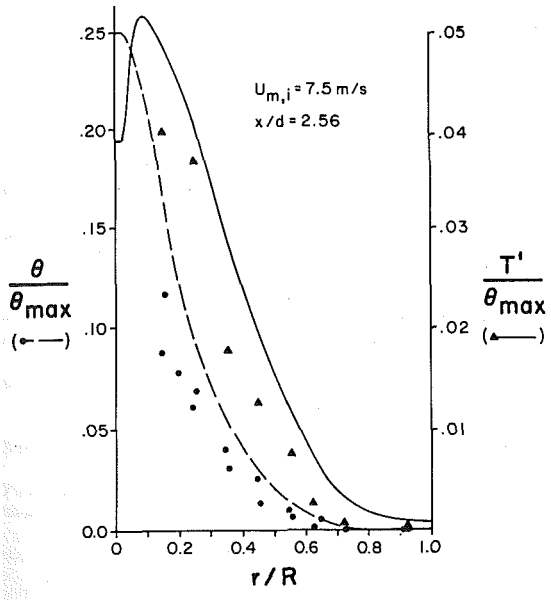

Fig. 5 Radial profiles of time-mean and RMS temperature fluctuation

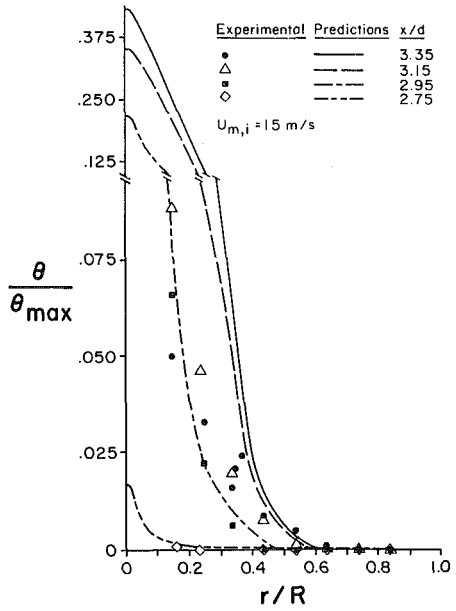

Fig. 6 Radial profiles of time-mean temperature (15 m/s)

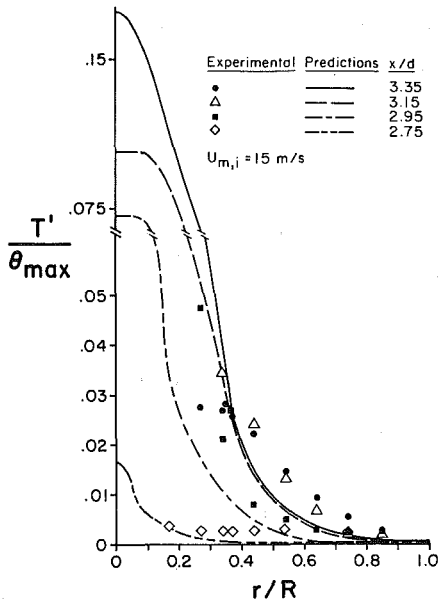

Fig. 7 Radial profiles of RMS temperature fluctuation

before. The reason is that the momentum of the main flow is only 25 percent of that of the high velocity case.

The Kinetic Energy of Turbulence. Figure 4 displays the predicted distribution of $(u^2/U^2)_{C.L.}$ for the cold and heated flows of $U_{m,i}$ = 7.5m/s. The value of u^2 was approximated as (2/3)k. In the cold flow, the first peak of the turbulence intensity along the centerline is associated with the boundary of the recirculation zone at $x/d \approx 2.5$. The second peak (at $x/d \approx 3.4$) is just upstream of the jet exit ($x/d \approx 3.54$) where the boundary of the small diameter (1.3mm) jet with large negative velocity interacts with the much slower mainstream. At that station, the production of k reaches a maximum at the shear layer between the two flows and is then transported to the axis. It is seen that the first peak in the heated flow is farther from the jet exit than in the cold flow. This is consistent with the discussion of the mean velocity results. The experimental values of $(u^2/U^2)_{C.L.}$ at the three axial locations are shown for both the cold and heated flows. These locations are outside the recirculation zone (i.e., farther from the jet exit). These values are in good agreement with the predictions.

The Time-Mean and RMS Temperature. Figure 5 shows the radial profiles of Θ/Θ_{max} and T'/Θ_{max} at x/d = 2.56 for the 7.5 m/s flow. Because of interference between the probe and jet body, measured values were not obtained at radial locations of r/R less than 0.15. The predictions depict a peak at r/R of 0.1 in the T'/Θ_{max} distribution; this is associated with the steep gradient in Θ/Θ_{max} at that radial location. In the outer region, the predictions are in fair agreement with measurements.

Figures 6 and 7 show the radial profiles of Θ/Θ_{max} and $T'\Theta_{max}$ at four axial locations for the 15 m/s flow. The axial and radial thermal extent of the heated jet is shown on both figures. It is interesting to note that, as expected, the radial extent of the temperature fluctuations is larger than that of the mean temperature at all the four stations.

The mean temperature is well predicted at stations farther from the jet exit and overpredicted near it. This may be attributed to overpredicted turbulent diffusion coefficients which could be due to low predicted values of ϵ or due to the use of a constant σ_H.

At the station x/d = 2.95, the predicted Θ/Θ_{max} is in excellent agreement with the experimental data. However, at the same station, the temperature fluctuations are underpredicted. This may suggest a lower value of C_{T2} or a high value of C_{T1} than those employed in the present predictions,

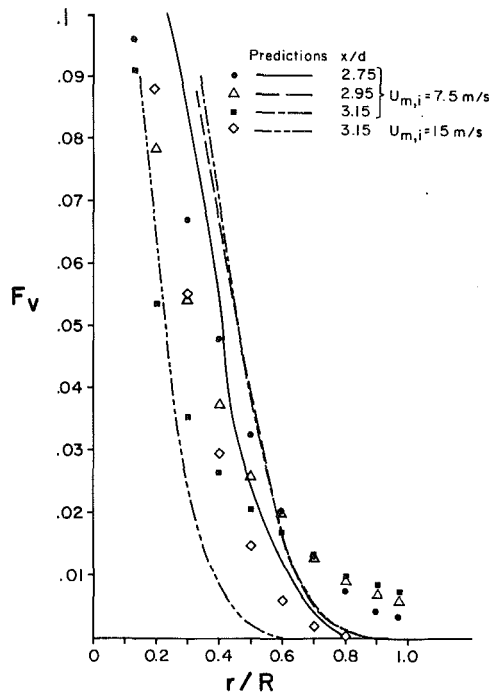

Fig. 8 Radial profiles of time-mean CO volume fraction

but an examination of Fig. 5 would run contrary to that suggestion.

It should be mentioned here that the transport equation for the mean square fluctuation of a scalar quantity (10) has been validated for turbulent free jets [17] and for confined turbulent recirculating flows [18]. The same equation (with both the values of C_{T2} of 2. and 1.4) did not predict accurately the measured values of RMS temperature fluctuations under the experimental conditions of this study. This stresses the need to solve a transport equation for the dissipation of the temperature fluctuation.

The Time-Mean CO Concentration. Figure 8 exhibits the measured and predicted radial profiles of CO volume-fraction (F_v) at three stations for the 7/5 m/s flow and at one station for the 15 m/s flow.

For the 7.5 m/s flow, F_v is overpredicted near the axis and underpredicted in the outer region ($r/R > .5$). However, F_v is underpredicted for the 15 m/s flow. Again, this points out the need for a closer look at the ϵ equation and for a distribution of σ_F instead of the constant value used in the present predictions.

Conclusions

The present contribution provides detailed measurements of velocity, temperature, and concentration in a turbulent inert recirculating confined flow with the objective of validating current mathematical models of turbulence.

Although fair agreement is obtained between the measured and predicted mean velocity field, discrepancies occur between the experimental data and the predicted time-mean temperature, time-mean concentration and RMS temperature fluctuation.

The need exists for a closer examination of the ϵ equation and the assumption of the constant turbulent Prandtl and Schmidt numbers. One such example is a recent development of the k-ϵ model [19].

In order to improve the predicted distribution of the temperature fluctuation a transport equation for the dissipation rate of this fluctuation must be solved.

Acknowledgments

This study was performed at the UCI Combustion Laboratory and sponsored by the Air Force Office of Scientific Research (Grant No. AFOSR-78-3586). The U. S. Government is authorized to reproduce and distribute reprints for government purposes notwithstanding any copyright notation hereon. Support for one of the authors (J. C. LaRue) was obtained from a NSF grant, ENG-78-15712 and NASA grant, L-NSG-3219.

References

1 Elghobashi, S. C., *Studies in Convection,* Vol. 2, edited by B. E. Launder, Academic Press, 1977, p. 141.

2 Peck, R. E., and G. S. Samuelsen, "Analytical and Experimental Study of Turbulent Methane Fired Backmixed Combustion," *AIAA Journal,* Vol. 15, No. 5, 1977, p. 730.

3 Khalil, E. E., D. B. Spalding, and J. H. Whitelaw, "The Calculation of Local Flow Properties in 2-D Furnaces," *Int. Journal of Heat and Mass Transfer,* Vol. 18, 1975, p. 775.

4 Wuerer, J., and G. S. Samuelsen, "Predictive Modeling of Back-mixed Combustor Flows: Mass and Momentum Transport," AIAA 79-0215, presented at the 17th Aerospace Sciences Meeting, New Orleans, Jan. 1979.

5 Peck, R. E., and G. S. Samuelsen, "Eddy Viscosity Modeling in the Prediction of Turbulent, Backmixed Combustion Performance," Sixteenth Symposium (International) on Combustion, The Combustion Institute, 1977, p. 1675.

6 Wyngaard, J. C., "Spatial Resolution of a Resistance Wire Temperature Sensor," *Phy. Fluids,* Vol. 14, 1971, p. 2052.

7 Bremhorst, K. and D. B. Gilmore, "Influence of End Conduction on the Sensitivity & Stream Temperature Fluctuations of a Hot-Wire Anemometer," *Int. J. Heat Mass Transfer,* Vol. 21, 1978, p. 145.

8 Millon, F., P. Paranthoen, and M. Trinite, "Influence des Echanges Thermiques Endre le Capteur et ses Supports sur la Measure des Fluctuations de Temperatures dans un Ecoulement Turbulent," *Int. J. Heat Mass Transfer,* Vol. 21, 1978, p. 1.

9 Larsen, S. E., and J. Højstrup, "Spatial and Temporal Resolution of a Resistance Wire Sensor," *J. Atmos. Sci,* (submitted for possible publication).

10 LaRue, J. C., T. Deaton, and C. H. Gibson, "Measurements of High Frequency Turbulent Temperature," *Rev. Sci. Instrum.,* Vol. 46, No. 5, 1975, pp. 757–764.

11 Launder, B. E., and D. B. Spalding, "The Numerical Computation of Turbulent Flows," *Computer Methods in Applied Mechanics and Engineering,* Vol. 3, 1974, p. 269.

12 Spalding, D. B., "Concentration Fluctuations in a Round Turbulent Free Jet," *Chem. Eng. Sc.,* Vol. 26, 1971, p. 95.

13 Launder, B. E., and D. B. Spalding, "Turbulence Models and their Experimental Verification," Lectures for Post Experience Course held at Imperial College, Apr. 1973, p. 11.5.

14 Gibson, C. H., and W. H. Schwarz, "The Universal Equilibrium Spectra of Turbulent Velocity and Scalar Fields," *Journal of Fluid Mechanics,* Vol. 16, 1963, p. 365.

15 Launder, B. E., Private Communication, Nov. 1973.

16 Patankar, S. V., and D. B. Spalding, "A Calculation Procedure for Heat, Mass and Momentum Transfer in Three Dimensional Parabolic Flows," *Int. J. Heat Mass Transfer,* Vol. 15, 1972, p. 1787.

17 Lockwood, F. C. and A. S. Naguib, "The Prediction of the Fluctuations in the Properties of Free Round Jet, Turbulent Diffusion Flames, *Combustion and Flame,* Vol. 24, 1975, p. 109.

18 Elghobashi, S. E., W. M. Pun, and D. B. Spalding, "Concentration Fluctuations in Isothermal Turbulent Confined Jets," *Chem. Eng. Sc.,* Vol. 32, 1977, p. 161.

19 Hanjalić, K., B. E. Launder, and R. Schiestel, "Multiple-Time-Scale Concepts in Turbulent Transport Modeling," Proceedings of Second Symposium on Turbulent Shear Flows," July 1979, London.